Astronomy
&
Astrophysics

A multi-wavelength study of the IRAS Deep Survey galaxy sample

II. The far-IR properties

P. Mazzei[1], A. della Valle[1,2], and D. Bettoni[1]

[1] INAF, Padova Astronomical Observatory, Vicolo dell'Osservatorio 5, Padova 35128, Italy
e-mail: [paola.mazzei;antonio.dellavalle;daniela.bettoni]@oapd.inaf.it
[2] Department of Astronomy, Padova, Italy

ABSTRACT

Context. The luminosity function (LF) is a basic tool in the study of galaxy evolution since it constrains galaxy formation models. The earliest LF estimates in the IR and far-IR spectral ranges seem to suggest strong evolution. Deeper samples are needed to confirm these predictions. We have a useful IR data set, which provides a direct link between IRAS and ISO surveys, and the forthcoming deeper Spitzer Space Telescope and Akari cosmological surveys, to address this issue.
Aims. This data set allows us to derive the 60 μm local LF to sensitivity levels 10 times deeper than before, to investigate evolutionary effects up to a redshift of 0.37, and, using the 60/15 μm bi-variate method, to analyze the poorly known 15 μm local LF of galaxies.
Methods. We exploited our ISOCAM observations of the IRAS Deep Survey (IDS) fields, to correct the 60 μm fluxes for confusion effects and observational biases. We find indications of a significant incompleteness of the IDS sample, still one of the deepest far-IR selected galaxy samples, below $\simeq$80 mJy. We have reliable identifications and spectroscopic redshifts for 100% of a complete subsample comprising 56 sources with $S(60\,\mu\text{m}) > 80$ mJy.
Results. With our spectroscopic coverage we construct the 60 μm LF for a sample complete down to 80 mJy. This LF extends over three orders of magnitude in luminosity, from 9 up to more than 12 in $\log(L_{60}/L_\odot)$. Despite the fact that the redshift range of our sample exceeds $z = 0.3$, the $V/V_{\max}$ test gives $\langle V/V_{\max}\rangle = 0.51 \pm 0.06$, consistent with a uniform distribution of sources. A more direct test, whereby the LF was measured in each of four different redshift intervals, does not point out any signature of evolution. On the other hand, the rest-frame 15 μm local LF we derive, extends up to $\log(L_{15}/L_\odot) = 12$ and predicts 10 times more sources at $\log(L_{15}/L_\odot) = 11$ than before.

Key words. galaxies: evolution – galaxies: ISM – galaxies: luminosity function, mass function

1. Introduction

Understanding how galaxies form and evolve is a key goal of modern physical cosmology. A fundamental observable of galaxies is their luminosity function (LF), which has long been used to constrain galaxy formation models and to quantify star formation and evolution both in luminosity and in density. The IR and far-IR spectral ranges are the best to deepen our knowledge of this subject since they trace the star formation that is responsible for galaxy formation. In particular, several satellite missions in the past (IRAS and ISO) and in the present (Spitzer, Akari) provided and will provide data that will be complementary for a detailed study of the LFs in such spectral domains.

The earliest IR estimate of the LFs, derived from the IRAS data (Rowan-Robinson et al. 1987; Saunders et al. 2000), indicated strong evolution, so that LF increases with redshift $\propto (1 + z)^{3\pm1}$. Moreover, deep surveys at 15 μm carried out with ISO (i.e., Elbaz et al. 1999; Flores 1999; Lari et al. 2001; Metcalfe et al. 2003) seem to require strong evolution of 15 μm sources (Lagache et al. 2005, and references therein). Several evolutionary models were developed to explain these results (e.g., Franceschini et al. 2001; Rowan-Robinson 2001) and to fit the IR/submillimiter source counts with different degrees of success. Nevertheless, none of them is based on a local LF obtained from 15 μm data, since the only available data until recently came from IRAS 12 μm photometry (Rush et al. 1993;

Xu 1998; Fang et al. 1998). The first attempt to build up the 15 μm LF of a NEPR subsample was made by Xu (2000). However, he said that it must be considered as a preliminary work because: i) the sample of galaxies used is an incomplete sample; ii) there is a possible misidentification between the sources in the 60 μm redshift survey of Ashby et al. (1996) and the 15 μm sources in his work (see della Valle et al. 2006, for more details); and iii) the model used to interpret the data treated all IR galaxies as a single population.

Our IDS/ISOCAM sample overcomes all these issues. It comprises a complete, 60 μm selected sample of 56 galaxies in the North Ecliptic Polar Region (NEPR), a subsample of the original 98 IRAS Deep Survey (IDS) fields (Hacking & Houck 1987). The IDS sample was defined by co-adding IRAS scans of the NEPR, representing more than 20 h of integration time (Hacking & Houck 1987). It comprises 98 sources with $S(60\,\mu\text{m}) > 50$ mJy over an area of 6.25 square degrees.

Mazzei et al. (2001) exploited ISOCAM observations (range 12–18 μm) of 94 IDS fields (Aussel et al. 2000), centered on the nominal positions of IDS sources, to correct the 60 μm fluxes for confusion effects and observational biases, finding indications of a significant incompleteness of the IDS sample below $\simeq$80 mJy. In della Valle et al. (2006), we presented spectroscopic and optical observations of candidate identifications of our ISOCAM sources. Combining such observations with those by Ashby et al. (1996), we have reliable identifications and

spectroscopic redshifts for 100% of the complete subsample comprising 56 sources with $S(60\,\mu m) > 80$ mJy. It is the deepest complete IRAS selected sample available and still one of the deepest complete far-IR selected samples. For comparison, the IRAS *Point Source Catalog* (hereafter PSC; Beichman et al. 1988) comprises about 250 000 IR sources with a completeness limit of 0.5 Jy at $60\,\mu m$ (Soifer et al. 1987). The deep ISOPHOT surveys, FIRBACK at $170\,\mu m$, (Puget et al. 1999; Dole et al. 2001), and ELAIS at $90\,\mu m$ (Oliver et al. 2000) are all complete down to about 100 mJy. Moreover, the $70\,\mu m$ Spitzer catalog of the 8.75 sq. deg. Bootes field is flux limited to 80 mJy (Dole et al. 2004) and the Spitzer extragalactic "main" First Look Survey, covering about 4 sq. deg., is complete to about 20 mJy at $70\,\mu m$ (cf. Fig. 2 of Frayer et al. 2006), but redshift measurements are available for a substantial fraction of sources (currently only 72%) merely for $S_{70\,\mu m} > 50$ mJy.

Thanks to our ISOCAM and optical/near-IR observations, our sample, which provides a direct link between the IRAS and ISO surveys, and the forthcoming deeper Spitzer Space Telescope and Akari cosmological surveys[1], is one of the far-IR selected complete samples with the larger spectral coverage. In addition to the ISOCAM and to the $60\,\mu m$ fluxes, most of our sources ($\simeq 70\%$) have $100\,\mu m$ fluxes, while the remaining 30% have upper limits, and several ($\simeq 40\%$) have $25\,\mu m$ fluxes from IRAS (Mazzei et al. 2001). Optical imaging has been already performed for 62.5% out of such a sample in at least one band, B or R, and for 34% in both the bands (della Valle et al. 2006); moreover, Two Micron All Sky Survey (2MASS) data are available for 68% of the sample and VLA observations for a large fraction of these sources are also available (Hacking et al. 1989).
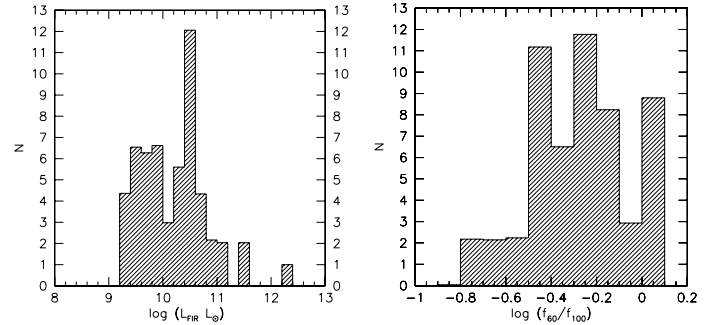
In this paper, which is the second step of our multi-wavelength approach devoted to the study of the evolution of a far-IR selected sample of galaxies on which numerous studies of the far-IR evolution of galaxies still rely, we derive the $60\,\mu m$ LF of such a sample. Our sample, ten times deeper in flux density than the PSC catalog, and thus less liable to be affected by the local density inhomogeneity, allows us to investigate evolutionary effects up to a redshift of 0.37, five times deeper than the PSCz catalog ($z \leq 0.07$, Saunders et al. 2000). Moreover, we use the bi-variate method to translate the $60\,\mu m$ LF to the poorly known $15\,\mu m$ LF. We will compare our results with the recent determination of the $15\,\mu m$ local LF obtained by Pozzi et al. (2004) using the available data on the southern fields, S1 and S2, of the ELAIS survey (Oliver et al. 2000).

The paper is organized as follows: Sect. 2 focuses on far-IR properties of our complete sample, Sect. 3 shows our derived $60\,\mu m$ LF, and Sect. 4 presents the $15\,\mu m$ LF based on the bi-variate $60/15\,\mu m$ method. In Sect. 5 there are our conclusions. Here and in the following we adopt: $\Lambda = 0.7$, $\Omega_b = 0.3$, $H_0 = 70$ km s^{-1} Mpc^{-1}.

2. The far-IR properties

Our complete sample comprises 56 IDS/ISOCAM sources. 25% out of these are beyond $z = 0.1$, 12.5% beyond $z = 0.15$, and


Fig. 1. *Left*: the rest-frame far-IR luminosity distribution of the IDS/ISOCAM sample of 56 galaxies. Here, as in Figs. 2–4, 7, 9, and 11, upper limits are taken into account by exploiting the Kaplan-Mayer estimator and by accounting for K-corrections and dust emission using evolutionary population synthesis models (see text). *Right*: the rest-frame distribution of the IRAS flux density ratio f_{60}/f_{100}, as revised in Mazzei et al. (2001), for the same sample.

only 5.3% at $z > 0.2$ (della Valle et al. 2006). Such a sample is deeper than previous estimates (Ashby et al. 1996), showing a tail extending up to $z = 0.375$, almost 4 Gyr in look-back time. Our morphological analysis (Bettoni et al. 2006) shows that, although 16% of our sources are multiple systems, unperturbed disk galaxies dominate the IDS/ISOCAM sample. One ULIRG, 3-53A, and two broad Hα emission line galaxies with AGN optical properties (i.e., 3-70A and 3-96A, see Bettoni et al. (2006) for more details) are also included in the complete subsample.

Figure 1 (left panel) shows the distribution of the far-IR luminosity (L_{FIR}, from 42.5 to 122.5 μm) of our sample, where $L_{FIR} = 4\pi D_L^2(\text{FIR})$, FIR $= 1.26 \times 10^{-14}(2.58 f_{60} + f_{100})$ W/m^2, and f_{60} and f_{100} are in Jy (Helou et al. 1988). In such a figure, as in the following ones, K-corrections were derived from evolutionary population synthesis models taking dust effects into account (Mazzei et al. 1995), luminosities were in units of solar bolometric luminosity, $L_\odot = 3.83 \times 10^{33}$ erg/s. Moreover, upper limits to flux densities were accounted for by exploiting the Kaplan-Meier estimator (Kaplan & Meier 1958). Calculations were carried out using the ASURV v 1.2 package (Isobe & Feigelson 1990), which implements methods presented in Feigelson & Nelson (1985) and in Isobe et al. (1986). The Kaplan-Meier estimator is a non-parametric, maximum-likelihood-type estimator of the "true" distribution function (i.e., with all quantities properly measured, and no upper limits). The "survivor" function, giving the estimated proportion of objects with upper limits falling in each bin, does not produce, in general, integer numbers, but is normalized to the total number. This is why non-integer numbers of objects appear in the histograms of our figures.

The far-IR luminosity of the IDS/ISOCAM sample extends over 3 orders of magnitude (Fig. 1, left panel) with a mean value, $\log(L_{FIR}) = 10.2$, slightly lower than the mode of the distribution, $\log(L_{FIR}) \approx 10.5$. This value is almost the same as that of the Revised IRAS $60\,\mu m$ Bright Galaxy Sample (Sanders et al. 2003), and of a normal spiral galaxy, like the Milky Way (Mazzei et al. 1992, and references therein). The ULIRG galaxy, 3-53A, emits the maximum far-IR luminosity of the sample, nearly 100 times higher than the median value. In the same figure (Fig. 1, right panel) we present the rest-frame distribution of the f_{60}/f_{100} flux density ratios for our sample. This ratio is a measure of the dust temperature, which gives information on the relative fraction of IR light from new and old star populations (Helou 1986; Mazzei et al. 1992). Its mean value, -0.3,

---
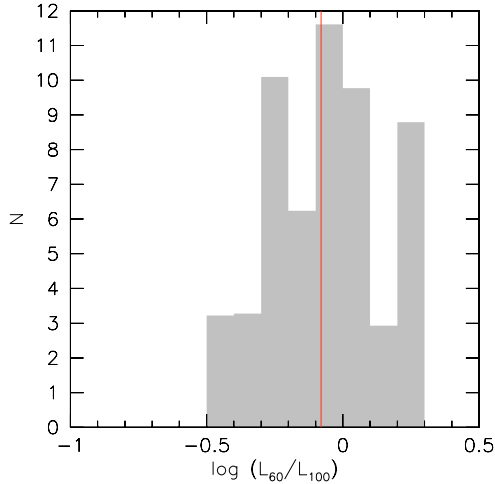
Fig. 2. The distribution of the rest-frame luminosity ratio, $\log L_{60}/L_{100}$, for our 56 IDS/ISOCAM sources; red continuous line corresponds to the value $\log L_{60}/L_{100} = -0.08$ (see text).

Fig. 3. The rest-frame far-infrared luminosity distribution for the IDS/ISOCAM sample of 56 galaxies. The separate distributions of *warm* (24 sources) and *cold* (32 sources) sub-populations are indicated with the (grey) open and (white) hatched histograms, respectively.

corresponds to a grain temperature of about 36 K, consistent with the value observed for the bulk of IRAS galaxies (Sanders et al. 2003; Soifer et al. 1987). The L_{60}/L_{100} ratio correlates with far-IR luminosity, as expected for the flux density ratio, f_{60}/f_{100}, but avoiding any redshift dependence, with the most luminous IRAS sources having the largest values of such a ratio (see Sanders & Miraleb 1996, and references therein). From the distribution of the rest-frame luminosity ratio, L_{60}/L_{100}, we derive a mean value of -0.08 (Fig. 2). We divide the sample into two subsamples separated about this mean, i.e., a *warm* subsample of 24 IDS/ISOCAM sources with $\log(L_{60}/L_{100}) \geq -0.08$, and a *cold* subsample of 32 objects having $\log(L_{60}/L_{100}) < -0.08$ (Rowan-Robinson & Crawford 1989). Figure 3 shows the far-IR luminosity distributions of *warm* and *cold* sources in our sample. *Warm* systems entail the overall luminosity range with a mode (mean) value, 10.45 (10.3), about 3 (1.5) times higher than that of *cold* sources.

We use the total far-IR luminosity to quantify the star formation rate (SFR). According to Chapman et al. (2000), $L_{TIR} = k \times$ *SFR* with k ranging from 1.5 to 4.2, in units of $10^9\ L_\odot\ M_\odot\ \mathrm{yr}^{-1}$, for Salpeter's IMF with upper and lower mass limits 100 $M_\odot$ and 0.1 $M_\odot$, respectively, and $L_{TIR} = 1.7 \times L_{60}$. We adopt $k = 4.2$ by comparing the SFR as defined above with the Hopkins et al. (2003) calibration. The more luminous 60 μm sources, i.e., those with higher SFRs, correspond to the more distant systems, 3-96 and 3-53, two *warm* sources (Fig. 4).

The dust temperatures suggest the presence of two galaxy populations: a spiral population with normal dust temperature (i.e., <36 K), mean SFR $\simeq$6 $M_\odot$/yr, mean far-IR luminosity, $\log(L_{FIR}) \simeq 10.1$, and mean redshift 0.075, together with a starburst population characterized by warm dust temperature (i.e., $\geq$36 K), mean SFR $\simeq$ 12 $M_\odot$/yr, mean far-IR luminosity, $\log(L_{FIR}) \simeq 10.3$, and mean redshift 0.1 (Fig. 5).
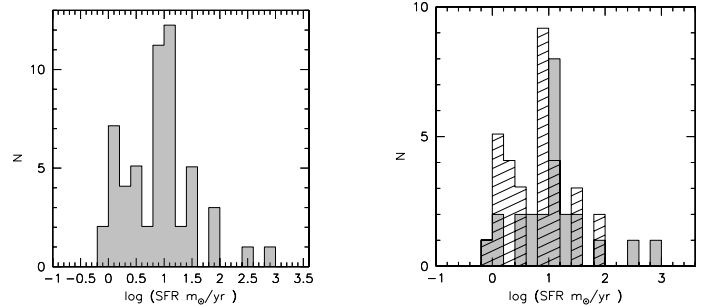
3. The 60 μm luminosity function

The observed flux S_ν is related to the rest-frame luminosity by:

$$L_\nu = 4\pi\ D_L^2\ S_\nu\ /k\ (L, z),\qquad (1)$$
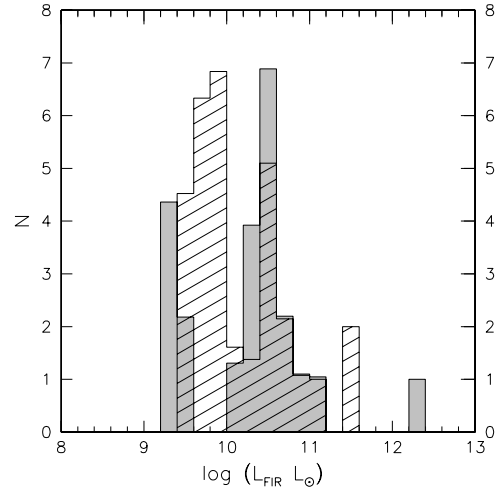
Fig. 4. *Left*: the SFR distribution for our sample of 56 sources. *Right*: the SFR distribution for *warm*, 24, and for *cold*, 32 sources, (grey) open and (white) hatched histograms respectively.

where D_L is the luminosity distance, computed according to our cosmological model (Sect. 1), and $k\ (L, z)$ is the K-correction defined as:

$$k\ (L, z) = \frac{(1 + z)\ L_{\nu(1+z)}}{L_\nu}.\qquad (2)$$

For the most distant galaxies ($z > 0.2$) the correction exceeds 20% of the luminosity. Figure 6 shows our derived 60 μm differential luminosity function, i.e., the co-moving number density of sources per logarithmic luminosity interval, $\phi(L_{60}, z)\Delta \log L_{60}$, where $L_{60} = \nu L_\nu$, calculated using the Schmidt-Eales $1/V_{max}$ estimator proposed by Schmidt (1968) and improved by Felten (1976) and Eales (1993). We assume Poisson errors, as tabulated by Gehrels (1986). L_{60}, i.e., the rest-frame luminosity, has been K-corrected as specified in Sect. 2.

According to the V/V_{max} test (Schmidt 1968), sources drawn from a population uniformly distributed in space should have a mean value of V/V_{max} equal to 0.5. Larger (smaller) values of V/V_{max} are the result of a strong increase (decrease) of the co-moving space density of sources with redshift. We find $\langle V/V_{max}\rangle = 0.51 \pm 0.06$, consistent with a uniform distribution of sources. The IDS/ISOCAM sample is ten times deeper in flux density than the PSCz catalog and 100 times deeper than the IRAS 60 μm Bright Galaxy Sample (Sanders et al. 2003), but no signatures of evolution arise from our sample.
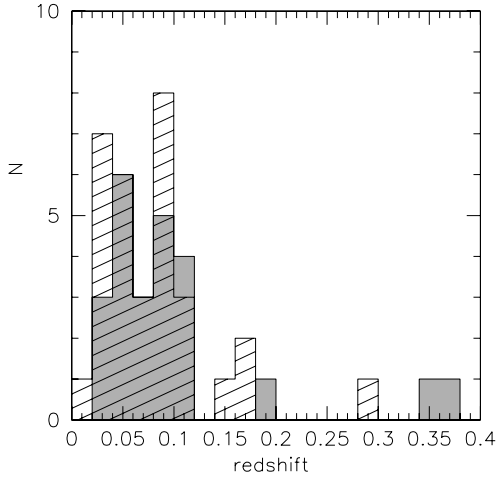
Fig. 5. The redshift distribution for *warm*, 24, and for *cold*, 32 sources, (grey) open and (white) hatched histograms, respectively.
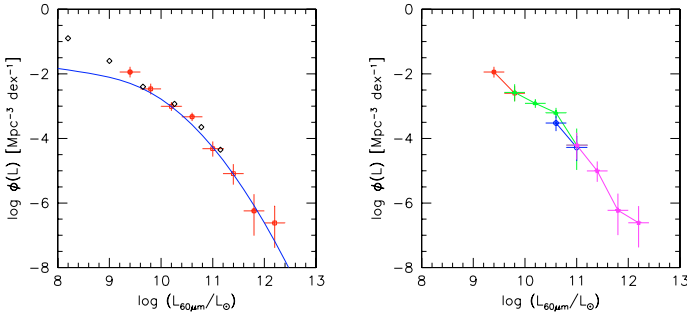
Fig. 6. *Left*: the rest–frame 60 μm LF for our sample of 56 IDS/ISOCAM sources (red open squares) compared with LF of IRAS PSCz galaxies from Takeuchi et al. (2003, 2004; blue continuous line) and with LF of Spitzer extragalactic First Look Survey from Frayer et al. (2006) (black open diamonds). The bin size is $\Delta \log L_{60} = 0.4$. *Right*: LF split into different redshift bins: asterisks (red) for $z < 0.05$, triangles (green) for $0.05 \leq z < 0.010$, open circles (blue) for $0.010 \leq z < 0.015$, and stars (magenta) for $z > 0.15$.

The LF we derive is in good agreement with previous works based on the IRAS PSC (Saunders et al. 1990; Takeuchi et al. 2003, 2004). Takeuchi et al. (2003, 2004) revised the work by Saunders et al. (1990) by enlarging their galaxy sample to 15 411 galaxies from the PSCz (Saunders et al. 2000) with a flux limit of 600 mJy and a redshift range between 0 and 0.07. Their analytic fit, shown in Fig. 6, is based on the same parameterization as Saunders et al. (1990):

$$\phi(L_\nu) = \phi_* \left(\frac{L_\nu}{L_*}\right)^{1-\alpha} \exp\left[-\frac{1}{2\sigma^2} \log_{10}^2\left(1 + \frac{L_\nu}{L_*}\right)\right] \qquad (3)$$

with parameters: $\alpha = 1.23 \pm 0.04$, $L_* = (4.34 \pm 0.86) \times 10^8 h^{-2} L_\odot$, $\sigma = 0.724 \pm 0.01$, and $\phi_* = (2.60 \pm 0.30) \times 10^{-2} h^3$ Mpc^{-3} (Takeuchi et al. 2003, 2004).

Our results extend over three orders of magnitude in luminosity, from $\log(L_{60}/L_\odot) \simeq 9$ up to more than 12. In the range where the samples overlap, our findings agree with the recent determination by Frayer et al. (2006, diamonds in Fig. 6), based on a complete sample of 58 sources with $S_{70} > 50$ mJy and $z < 0.3$, drawn from the *Spitzer extragalactic First Look Survey*. Despite the fact that the redshift range exceeds $z = 0.3$, our LF does not show any evidence of evolution. A more direct test for evolution has been performed by computing LF in four different redshift

Table 1. The 60 μm luminosity function: V/V_{max} in different redshift bins.

Redshift bin	V/V_{max}
$0.00 \leq z < 0.05$	0.490 ± 0.04
$0.05 \leq z < 0.10$	0.471 ± 0.08
$0.10 \leq z < 0.15$	0.444 ± 0.07
$z > 0.15$	0.315 ± 0.08

bins assuming no evolution (see Fig. 6, right panel, and Table 1). The results are fully consistent with this assumption.

4. The 15 μm luminosity function

Deep surveys at 15 μm carried out using ISO (i.e., Elbaz et al. 1999; Flores 1999; Lari et al. 2001; Metcalfe et al. 2003) seem to require strong evolution of 15 μm sources starting from redshift 0.5 (see Lagache et al. 2005 and references therein). Several evolutionary models were developed to explain these results (e.g., Franceschini et al. 2001; Rowan-Robinson 2001), trying to fit IR/submillimeter source counts with different degrees of success. Nevertheless, none of them is based on a local LF obtained from 15 μm data since the only available data until few years ago came from IRAS 12 μm photometry (Rush et al. 1993; Xu 1998; Fang et al. 1998).

A first attempt to build up the 15 μm LF of a NEPR subsample was made by Xu (2000), using the bi-variate method to translate the 60 μm local LF of IRAS galaxies (Saunders et al. 1990) to 15 μm. Its sample comprises 64 sources detected both at 60 μm (Hacking & Houck 1987) and at 15 μm (Aussel et al. 2000), with redshifts measured by Ashby et al. (1996). Xu fitted the result obtained (see its Table 2 and Fig. 3), with a pure luminosity evolution model $L \propto (1 + z)^{4.5}$. Nevertheless he said that it must be considered as a preliminary work, as discussed in Sect. 1.

A recent determination of the 15 μm local LF was made by Pozzi et al. (2004) using the available data on the southern fields, S1 and S2, of the ELAIS survey (Oliver et al. 2000). Their data sample entails 150 galaxies with redshift $z \leq 0.4$, excluding sources classified as AGNs (both type one and type two). The 15 μm LF was calculated with a parametric maximum likelihood method. Pozzi et al. (2004) separate spirals from starbursts using optical/mid-IR ratios, assuming that starbursts are the more mid-IR luminous galaxies with, on average, larger $\log(L_{15}/L_R)$ ratios. They estimate the 15 μm local LF in the range $7.8 \leq \log(L/L_\odot) \leq 10.6$. Their findings are that the 15 μm LF of spirals is consistent with no evolution ($\langle V/V_{max}\rangle = 0.55 \pm 0.03$), but that the value $\langle V/V_{max}\rangle = 0.64 \pm 0.03$ measured for the starbursts suggests that this population is in fact evolving.

4.1. The bi-variate method

Since our sample is flux limited at 60 μm, but not at 15 μm, we used the bi-variate method to calculate the 15 μm LF of our sample. It was obtained by a convolution of the 60 μm LF with the $\log(L_{15}/L_{60})$ distribution:

$$\phi(\log L_{15}) = \int \phi(\log L_{60})\, P(\log(L_{15}/L_{60}))\, d(\log L_{60}), \qquad (4)$$

where $P(\log(L_{15}/L_{60}))$ is the conditional probability function that gives the distribution of $\log(L_{15})$ around the mean 15 μm luminosity $\langle \log(L_{15})\rangle$ at a given 60 μm luminosity $\log(L_{60})$.

Table 2. Coefficients and parameters describing the distribution function, Pearson I curve of our sample.

Case	y_0	a_1	a_2	m_1	m_2	Mode	Mean	σ	Skew	Kurt	χ^2_ν
All	82.8	12.9	0.43	83.3	2.72	–0.60	–0.69	0.24	0.52	0.52	0.77
σ_p	16.5	1.56	0.04	10.2	0.39	0.04					

Table 3. Parameters describing the LF of our sample.

Case	$\phi_*/10^{-3}$ Mpc^{-3}	$L_*/10^8 L_\odot$	α	σ
All	$5.32 \pm .40$	$2.00 \pm .18$	$1.241 \pm .021$	$0.748 \pm .010$
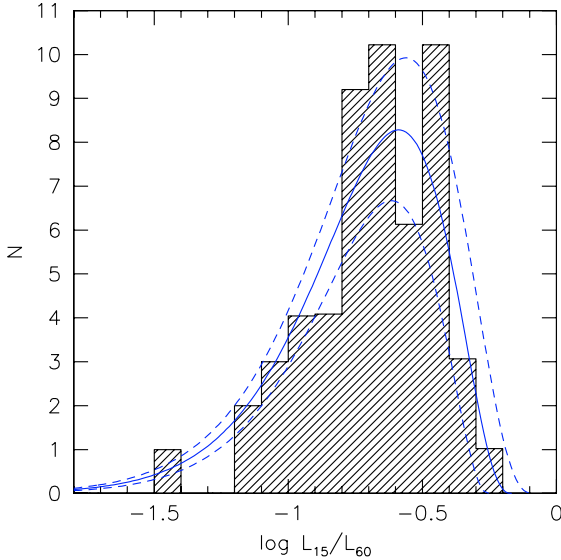
Fig. 7. Distribution of the $\log L_{15}/L_{60}$ ratio for 54 IDS/ISOCAM sources (see text). The bin size is $\Delta(\log L_{15}/L_{60}) = 0.1$. The fitting function is a type I Pearson whose parameters, optimized following the Levenberg-Marquardt method (see text), are reported in Table 2; dashed lines show the same curves with one σ error in the parameters.

The distribution per unit interval of the logarithm of the luminosity ratio is well described by type I Pearson's curves (Pearson 1924; Elderton & Johnson 1969):

$$y = y_0 \, (1 + x/a_1)^{m_1} \, (1 - x/a_2)^{m_2}, \qquad (5)$$

where $x = \log(L_{15}/L_{60})$, with $-a_1 \le x \le a_2$, and its origin is at the position of the peak of the distribution (*mode*). The values of the parameters are given in Table 2, together with the mean, the standard deviation σ, the skewness (μ_3^2/μ_2^3), and the kurtosis ($\mu_4/\mu_2^2 - 3$) of the distribution (μ_i is the ith moment about the mean). The quality of the fit is quantified by the value of χ^2 per degree of freedom (χ_ν), given in the last column and computed adopting the Levenberg-Marquardt method as implemented in Press et al. (1992); σ_p are the errors on the Pearson's parameters.

To perform these analyses we remove the sources 3-70 and 3-96 with AGN properties from our sample (see Sect. 2) and used the parametric solution of the 60 μm LF derived by Takeuchi et al. (2003, 2004), which agrees well with our results (see Sect. 3, Eq. (3)).

Table 3 lists the parameters defining our 15 μm local galaxy LF using the same parametric form as in Eq. (3) suggested by Pozzi et al. (2004). The Pozzi LF extends from 7.8 up to 10.6 in $\log(L_{15}/L_\odot)$, whereas our convolution extends over more than six orders of magnitude and 100 times deeper (Fig. 8). Our results agree with those by Pozzi et al. (2004) up to their
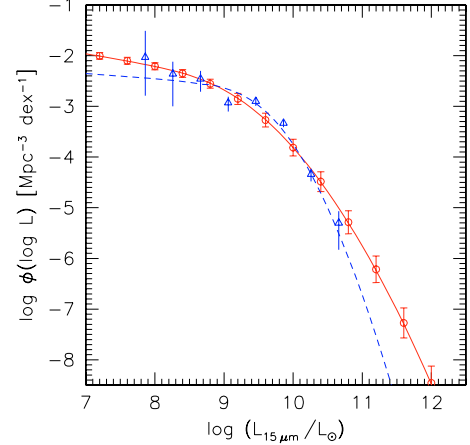
Fig. 8. The 15 μm differential LF (red continuous line) for the IDS/ISOCAM sample (54 sources) compared with that of Pozzi et al. (2004) (blue dashed line and open triangles). The error bars correspond to one σ error of the Pearson's curve parameters.

luminosity limit (10.6); however, beyond such a luminosity the two parametric LFs diverge so that at $\log(L_{15}/L_\odot) = 11$ we expect 10 times more sources than Pozzi et al. (2004).

4.2. Spiral and starburst populations

Our sample includes 22 galaxies with rest-frame *warm* L_{60}/L_{100} ratios and 32 galaxies with *cold* ratios, after excluding AGN (see Sect. 2). They define two different populations, starburst and spiral galaxies, respectively, as far as dust properties are concerned. Their distributions per unit interval of the logarithm of the luminosity ratios $\log(L_{15}/L_{60})$, shown in Fig. 9 (left panel), are fitted well by Pearson's curves whose parameters are in Table 4. Their 15 μm LF fits, i.e., Eq. (3), are in Fig. 9 (right panel), and the LF parameters are given in Table 5. We find that both populations contribute to the faint end of the LF. Spiral galaxies overcome starbursts by less than a factor of two. Such a factor is slightly reduced with luminosity, from 1.8 at $\log(L_{15}/L_\odot) = 8$ to 1.3 at $\log(L_{15}/L_\odot = 11.8)$. Our results differ from those of Pozzi et al. (2004), in particular predictions concerning starburst population. However, they used optical/mid-IR ratios instead of far-IR ratios to disentangle starbursts and spirals, assuming that starbursts are the more mid-IR luminous galaxies with, on average, larger $\log(L_{15}/L_R)$ ratios.

To investigate this point further, we repeated our analysis using the same criterion as Pozzi et al. (2004) to discriminate starbursts from spirals. We used the APS catalog (http://aps.umn.edu) R-band magnitudes for the 37.5% of our sample galaxies that lacked them (see Sect. 1), applying a correction of -0.75 mag to bring the APS zeropoint into agreement with our own common sources. Figure 10 shows the rest-frame L_{15}/L_R ratios vs. L_{15} luminosity. From a least-square-fitting procedure we find:

$$L_{15}/L_R = (0.64 \pm 0.04) \times L_{15} - (6.67 \pm 0.43) \qquad (6)$$

Table 4. Coefficients and parameters describing the distribution functions, Pearson I curves, of starburst and spiral populations.

Case	y_0	a_1	a_2	m_1	m_2	Mode	Mean	σ	Skew	Kurt	χ^2_ν
Starbursts	35.7	4.30	0.14	9.11	0.25	−0.39	−0.70	0.25	1.99	2.39	1.70
σ_p	12.3	1.55	0.02	3.56	0.18	0.002					
Spirals	43.2	1.47	0.32	4.43	0.19	−0.64	−0.64	0.23	0.05	−0.84	0.77
σ_p	11.6	0.58	0.01	1.89	0.11	0.01					

Table 5. Parameters describing the LFs of starburst and spiral populations.

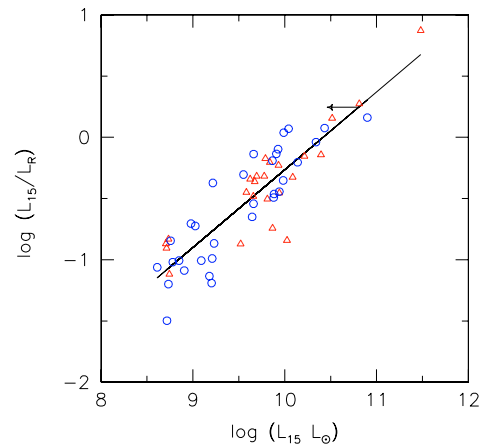| Case	$\phi_*/10^{-3}$ Mpc^{-3}	$L_*/10^8\,L_\odot$	α	σ
Starbursts	1.89 ± .03	2.96 ± .03	1.275 ± .001	0.740 ± .015
Spirals	3.36 ± .07	2.21 ± .07	1.236 ± .006	0.739 ± .027
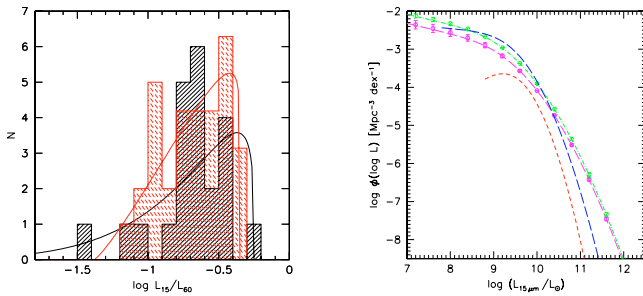
Fig. 9. *Left*: distribution of the $\log L_{15}/L_{60}$ ratios for starbursts (black continuous line), 22 sources, and spirals (red dashed line), 32 sources, selected on the basis of their far-IR colors. The bin size is $\Delta(\log L_{15}/L_{60}) = 0.1$ and the parameters of the fitting functions, type I Pearson curves, are in Table 4 together with one σ errors. *Right*: the contribution of such galaxy populations to the rest-frame 15 μm LF (see Table 5): starbursts (magenta long-dashed dotted line) and spirals (green dot-dashed line). Results are compared with those by Pozzi et al. (2004): starbursts (red short-dashed line) and spirals (blue long-dashed line).

Fig. 10. The behavior of the $\log L_{15}/L_R$ ratio for *warm* sources (24, red triangles), and for *cold* sources (32, blue open circles) of IDS/ISOCAM sample; the continuous line corresponds to the least-square fit (see Eq. (6)).

with a dispersion of 0.20 dex. Our fit is steeper, 0.64 instead of 0.5, than that of Pozzi et al. (2004). Following Pozzi et al. (2004), we assume $L_{15}/L_R = -0.4$ to be the nominal separation between spiral and starburst populations. *Warm* and *cold* galaxies, selected on the basis of their far-IR colors, are mixed in Fig. 10. Such a criterion selects different galaxies in both the populations. Now there are 30 spirals and 24 starbursts in our sample. The distributions per unit interval of the logarithm of their luminosity ratios $\log(L_{15}/L_{60})$, are fitted again by type I Pearson's curves (Fig. 11, left panel) whose parameters are in Table 6. Table 7 shows those of their 15 μm LF fits (Fig. 11, right panel). Both such populations contribute to the faint end of the LF. The space densities of starbursts are just slightly greater than those of spiral galaxies.

5. Conclusions

Combining our observations (della Valle et al. 2006) with those by Ashby et al. (1996), we have reliable identifications and spectroscopic redshifts for 100% of the complete far-IR selected sub-sample comprising 56 IDS sources with $S_{60} > 80$ mJy (Mazzei et al. 2001). The redshift distribution shows a tail extending up to $z \simeq 0.37$, in particular $\simeq 26\%$ of the sources have redshifts $z > 0.1$.

To fully exploit the potential of this sample, ten times deeper than the IRAS PSC, thus less liable to the effect of local density inhomogeneity, for investigating galaxy evolution, we

calculate the 60 μm LF using the $1/V_{\max}$ method. Current estimates are based on rather shallow samples. Even though our sample is five times deeper in redshift than the PSCz (Saunders et al. 2000) used by Takeuchi et al. (2003), our LF agree with their determination (Takeuchi et al. 2003, 2004) and with that by Frayer et al. (2006) based on a complete sample of galaxies with $S_{70} > 50$ mJy drawn from the Spitzer *extragalactic First Look Survey*. Despite the fact that our redshift range exceeds $z = 0.3$, and our 60 μm LF extends up to $\log L_{60} = 12$, whereas that by Frayer et al. (2006) up to $\log L_{60} \simeq 11$, does not show any evidence of evolution. The $V/V_{\max}$ test gives a value consistent with a uniform distribution ($V/V_{\max} = 0.51 \pm 0.06$). Moreover, a more direct test for evolution has been performed by splitting the LF in different redshift bins assuming no evolution. The results are fully consistent with this assumption.

We present the bi-variate 15 μm LF, one of the few determinations based on ISO data, by convolving the 60 μm LF with the luminosity ratio distribution, L_{15}/L_{60} of our sample. This extends to luminosity 100 times higher than before. Our result agrees with the recent determination by Pozzi et al. (2004) in the common range of luminosity, i.e., from 7.8 up to 10.6 in $\log(L_{15}/L_\odot)$. However, above $\log(L_{15}/L_\odot) = 10.6$, the two parametric LFs diverge so that at $\log(L_{15}/L_\odot) = 11$ we expect 10 times more sources than Pozzi et al. (2004). To investigate the role of galaxy populations on such a result, we disentangle starbursts and spirals on the basis both of their far-IR dust temperature, and of their L_{15}/L_R ratios, as assumed by Pozzi et al. (2004). Such criteria select galaxies with different dust

Table 6. Coefficients and parameters describing the distribution functions, Pearson I curves, of starburst and spiral populations.

Case	y_0	a_1	a_2	m_1	m_2	Mode	Mean	σ	Skew	Kurt	χ_ν^2
Starbursts	35.11	11.5	0.62	61.2	3.45	−0.63	−0.74	0.29	0.50	0.56	0.86
σ_p	10.7	2.29	0.12	12.3	0.74	0.11					
Spirals	60.3	10.0	0.33	47.8	0.94	−0.60	−0.67	0.21	0.41	−0.34	1.03
σ_p	13.0	2.61	0.13	12.6	0.47	0.11					

Table 7. Parameters describing the LF of starburst and spiral populations.

Case	$\phi_*/10^{-3}$ Mpc^{-3}	$L_*/10^8\,L_\odot$	α	σ
Starbursts	3.82 ± .62	1.81 ± .45	1.245 ± .048	0.761 ± .028
Spirals	2.92 ± .88	2.29 ± .85	1.234 ± .084	0.742 ± .037
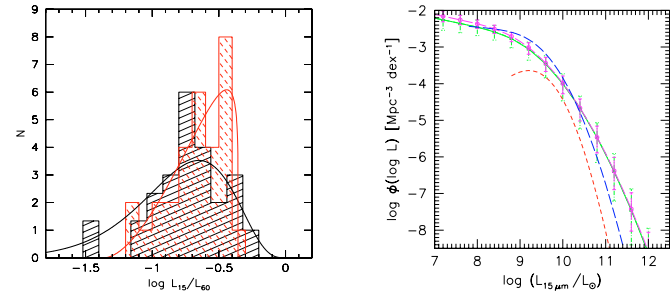
Fig. 11. *Left*: the distribution of the $\log L_{15}/L_{60}$ ratio for starbursts (black continuous line), 24 sources, and for spirals (red dashed line), 30 sources, selected with the same criterion as Pozzi et al. (2004). The bin sizes are $\Delta(\log L_{15}/L_{60}) = 0.12$ and 0.1, respectively. The parameters of the fitting functions, type I Pearson curves, are in Table 6. *Right*: the contribution of such galaxy populations to the rest-frame 15 μm LF (see Table 7): starbursts (magenta long-dashed dotted line) and spirals (green dot-dashed line). Our results are compared with those by Pozzi et al. (2004): starbursts (red short-dashed line) and spirals (blue long-dashed line).

properties, as we point out in Sect. 4.2. Nevertheless, we find that both galaxy populations contribute to the faint end of the rest-frame 15 μm LF, even though we adopt the same criterion as Pozzi et al. (2004). Moreover, in this case, above $\log(L_{15}/L_\odot) = 9$ our findings are that starbursts and spirals give almost the same contribution to the mid-IR LF, whereas Pozzi et al. (2004) predict that spirals contribute 5–10 times more than starbursts.

References

Aussel, H., Coia, D., Mazzei, P., et al. 2000, A&AS, 141, 257
Ashby, M., Hacking, P., Houck, J., et al. 1996, ApJ, 456, 428
Beichman, C. A., Neugebauer, G., Habing, H. J., et al. 1988, Infrared astronomical satellite (IRAS) catalogs and atlases. Volume 1: Explanatory supplement, NASA RP-1190
Bettoni, D., della Valle, A., Mazzei, P., et al. 2006, in prep.
Chapman, S. C, Scott, D., Syeidel, C. c, et al. 2000, MNRAS, 319, 318
della Valle, A., Mazzei, P., Bettoni, D., et al. 2006, A&A, 454, 453
Désert, F.-X, Boulanger, F., & Puget, J. L. 1990, A&A, 237, 215
Devriendt, J. E. G., & Guiderdoni, B. 2000, A&A, 363, 851
Dole, H., Rieke, G. H., Lagache, G., et al. 2004, ApJS, 154, 93
Eales, S. 1993, ApJ, 404, 51
Elbaz, D., Cesarsky, C. J., Fadda, D., et al. 1999, A&A, 351, L37
Elderton, W., & Johnson, N. 1969, Systems of Frequency Curves (Cambridge University Press)
Fang, F., Shupe, D., Xu, C., & Hacking, P. 1998, ApJ, 500, 693
Feigelson, E., & Nelson, P. 1985, ApJ, 293, 192
Flores, H., Hammer, F., Thuan, T. X., et al. 1999, ApJ, 517, 148
Felten, J. E. 1976, ApJ, 207, 700
Franceschini, A., Mazzei, P., de Zotti, G., & Danese, L. 1994, ApJ, 427, 140
Franceschini, A., Aussel, H., Cesarsky, C. J., et al. 2001, A&A, 378, 1
Frayer, D. T., Fadda, D., Yan, L., et al. 2006, ApJ, 131, 250
Gehrels, N. 1986, ApJ, 303, 336
Guiderdoni, B., Hiven, E., Bouchet, F. R., & Maffei, B. 1998, MNRAS, 295, 877
Hacking, P., & Houck, I. R. 1987, ApJS, 63, 311
Hacking, P., Beichman, C. A., Condon, J. J., & Houck, J. R. 1989, ApJ, 339, 12
Helou, G. 1986, ApJ, 311, L33
Helou, G., Khan, I., Malek, L., & Boehmer, L. 1988, ApJS, 68, 151
Hopkins, A., Miller, J., Nichol, R., et al. 2003, ApJ, 599, 971
Isobe, T., & Feigelson, E. 1990, Software Report: ASURV, The Pennsylvania State University, BAAS, 22, 917
Isobe, T., Feigelson, E., & Nelson, P. 1986, ApJ, 306, 490
Kaplan, E., & Meier, P. 1958, J. Am. Stat. Ass., 53, 457
Kennicutt, R. C. Jr. 1998, ARA&A, 36, 189
Kewley, L., Gelle, M., Jansen, R., & Dopita, M. 2002, ApJ, 124, 3135
Lagache, G., Puget, J.-L., & Dole, H. 2005, ARA&A, 43, 727
Lari, C., Pozzi, F., Gruppioni, C., et al. 2001, MNRAS, 325, 1173
Kauffmann, G., & Charlot, S. 1998, MNRAS, 297, L23
Mazzei, P., de Zotti, G., & Xu, C. 1992, A&A, 256, 45
Mazzei, P., Curir, A., & Bonoli, C. 1995, AJ, 422, 81
Mazzei, P., Aussel, H., Xu, C., et al. 2001, New Astr., 6, 265
Metcalfe, L., Kneib, J., McBreen, B., et al. 2003, A&A, 407, 791
Neugebauer, G., Habing, H. J., & van Duinen, R. 1984, ApJ, 278, L1
Oliver, S., Rowan-Robinson, M., Alexander, D., et al. 2000, MNRAS, 316, 749
Pearson, K. 1924, Tables for Statisticians and Biometricians (Cambridge University Press)
Pearson, C. P., Shibai, H., Matsumoto, T., et al. 2004, MNRAS, 347, 1113
Press, W. H., Teukolsky, S. A., Vetterling, W. T., & Flannery, B. P. 1992, Numerical Recipes in FORTRAN: The Art of Science Computing, second edition (Cambridge University Press)
Pozzi, S., Gruppioni, C., Oliver, S., et al. 2004, ApJ, 609, 122
Rowan-Robinson, M. 2001, ApJ, 549, 745
Rowan-Robinson, M., & Crawford, J. 1989, MNRAS, 238, 523
Rowan-Robinson, M., Helou, G., & Walker, D. 1987, MNRAS, 227, 589
Rowan-Robinson, M., et al. 1999, in The Universe as Seen by ISO, ESA SP-427
Rush, B., Malkan, M., & Spinoglio, L. 1993, ApJS, 89, 1
Sanders, D. B., & Miralbel, I. F. 1996, ARA&A, 34, 749
Sanders, D. B., Mazzarella, J. K., Kim, D., et al. 2003, AJ, 126, 1607
Saunders, W., Rowan-Robinson, M., Lawrence, A., et al. 1990, MNRAS, 242, 318
Saunders, W., Sutherland, W., Maddox, S., et al. 2000, MNRAS, 317, 55
Schmidt, M. 1968, ApJ, 151, 393
Soifer, B., Sanders, D., Madore, B., et al. 1987, ApJ, 320, 238
Takeuchi, T., Yoshikawa, K., & Ishii, T. 2003, ApJ, 587, L89
Takeuchi, T., Yoshikawa, K., & Ishii, T. 2004, ApJ, 606, L171
Xu, C. 2000, ApJ, 541, 134
Xu, C., Hacking, P., Fang, F., et al. 1998, ApJ, 508, 576